AD-A145 823 INTERACTION BETWEEN AN AIRFOIL AND A STREAMWISE VORTEX (U) ARMY RESEARCH AND TECHNOLOGY LABS MOFFETT FIELD CA AEROMECHANICS LAB K W MCALISTER ET AL. 27 JUN 84 1/1

UNCLASSIFIED F/G 20/4 NL

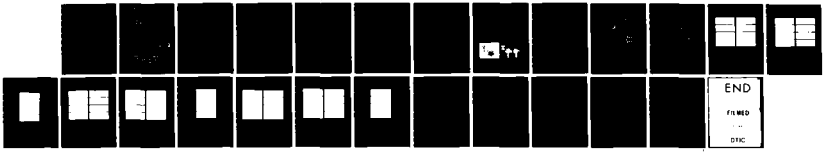

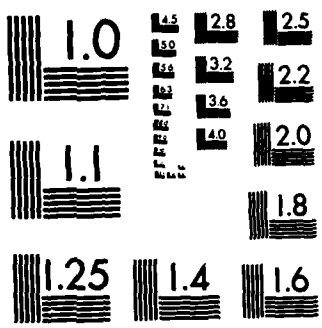

MICROCOPY RESOLUTION TEST CHART

AIAA'84

AIAA-84-1626

Interaction Between an Airfoil and a Streamwise Vortex

K.W. McAlister and C. Tung, Aeromechanics Laboratory, U.S. Army Research Technology Laboratories (AVSCOM)
NASA-Ames Research Center,
Moffett Field, CA

AIAA 17th Fluid Dynamics, Plasma Dynamics, and Lasers Conference

June 25-27, 1984/Snowmass, Colorado

INTERACTION BETWEEN AN AIRFOIL AND A STREAMWISE VORTEX

K. W. McAlister* and C. Tung†

Aeromechanics Laboratory, U.S. Army Research and Technology Laboratories (AVSCOM)
NASA Ames Research Center, Moffett Field, California

Abstract

The tip of a finite-span airfoil was used to generate a streamwise vortical flow, the strength of which could be varied by changing the incidence of the airfoil. The vortex that was generated traveled downstream and interacted with a second airfoil on which measurements of lift, drag, and pitching moment were made. The flow field, including the vortex core, was visualized in order to study the structural alterations to the vortex resulting from various levels of encounter with the downstream airfoil. These observations were also used to evaluate the accuracy of a theoretical model.

Nomenclature

c = chord length of generator airfoil

Re = Reynolds number based on downstream airfoil chord

α = angle of attack for downstream airfoil

$\tilde{\alpha}$ = angle of attack for generator airfoil

I. Introduction

The vortices that are generated by missiles, canards, wings, and rotor-blade tips often have a detrimental effect on the flow fields of other control or lifting surfaces. One of the most elementary models of this type of flow interaction is provided by the passage of a streamwise vortex near a downstream lifting airfoil. For an accurate calculation of this flow field, it is necessary to correctly account for 1) the time-varying viscous structure of the vortex; 2) the three-dimensional viscous flow over the airfoil, including the shedding of its own wake; and 3) the nonlinear path of the vortex resulting from its interaction with the airfoil. From the experimenters' point of view, the challenge is 1) to produce a fully developed, steady, and well-defined vortex in the flow, without the attendant wake of the generator, 2) to correctly scale the vortex-airfoil interaction, and 3) to provide suitable measurements in sufficient detail to meet the level of evaluation required.

The mathematical model for the impinging vortex has ranged in complexity from that of an inviscid-line vortex fixed along a rectilinear path, to a viscous-core vortex developing along an unprescribed path. Similarly, the mathematical model for the interacting airfoil has evolved from a simple lifting-line theory to a dense vortex-lattice representation.[1-3] Numerous experiments have been performed to assess the value of various combinations of these computational models, as well as to define the flow field and resultant loads on the airfoil during the interaction. These studies have shown that when details of the flow are required (such as airfoil pressure distribution) during a close vortex encounter (roughly within one core diameter), only the most comprehensive models are capable of providing calculations with acceptable accuracy. In those cases in which the vortex interaction is severe enough to cause separation on the airfoil, the choice of models must be narrowed to the few that include the boundary layer. Furthermore, the boundary-layer model must be three dimensional to account for the strong spanwise flow component caused by the interaction.[4] Recognition of the boundary layer is an important factor in determining the full effect of the vortex-airfoil interaction since vortex-induced separation on the airfoil has been found to substantially limit the extent of the induced loads.[5] Only recently have codes become available that are capable of treating the vortex interaction problem where flow separation is present,[6] and the results from one of these will be examined in light of the present experiment.

Although many noteworthy vortex interaction studies have preceded this investigation, some aspects of the problem have not been sufficiently addressed and therefore remain in question. Specifically, these questions concern the alterations to both the trajectory and stability of the vortex, as well as the overall performance of the airfoil resulting from the interaction. This subject can be most simply addressed by considering the case for a streamwise-oriented vortex encountering a two-dimensional lifting airfoil. Those questions pertaining to the vortex are 1) Does the path of the vortex essentially conform to the streamline pattern existing for the airfoil alone? 2) To what extent does the strength of the vortex influence its trajectory? and 3) Is proximity to the airfoil sufficient to cause an appreciable diffusion or breakdown of the vortex? Those questions regarding airfoil performance are 1) How does the presence of a nearby vortex (either passing above or below the airfoil) affect the airfoil stall? and 2) To what extent are the total prestall loads on the airfoil affected by a direct vortex impingement? These questions were to be addressed in the present experiment by visualizing the vortex and the airfoil boundary layer, along with direct measurements of airfoil lift, drag, and pitching moment.

In addition to obtaining certain physical insights into the subject of vortex-airfoil interactions, there was an interest in comparing the results of the experiment with the calculations of a promising mathematical model. This comparison would not only provide an opportunity to evaluate the accuracy of the model, but would also form the basis on which any refinements to the model are made.

*Research Scientist.
†Research Scientist. Member of AIAA.

II. Description of the Experiment

This study was conducted in the 4000-liter, closed-circuit water tunnel facility at the Aeromechanics Laboratory, Ames Research Center (Fig. 1). This was a particularly suitable facility for this investigation because of the ease of obtaining definitive visualizations of the vortex and the advantage of examining on-line the resultant loads on the airfoil during the interactions. The technique for visualizing the flow was based on the generation of minute hydrogen bubbles through electrolysis of a weak solution of sodium sulfate and water. Loads were measured directly by an external apparatus that served as both support and balance for the airfoil.

The airfoil selected for this study was a NACA 0012 having a two-dimensional planform of 10 cm (chord) by 21 cm (span). The test section measures 31 cm (height) by 21 cm (width), and the airfoil was positioned so that it spanned the width of the section to within 0.015 cm on either side. The airfoil was cast of an electrically nonconducting fiber resin, with platinum electrodes placed at nine chordwise locations along the upper surface. The bubbles that were generated at these electrodes were transported downstream by the fluid in the boundary layer and wake, thus enabling the thickness and eventual separation of the boundary layer to be observed.

The vortex was generated by placing a semispan airfoil at incidence in the free stream ahead of the NACA 0012 airfoil. The vortex generator was a NACA 0015 airfoil with a rectangular planform and a 5-cm chord (Fig. 2). Two vortex generators were constructed from an electrically nonconducting fiber resin. When installed, in turn, on the upper test section wall (Fig. 3), the tip of one generator would extend to the centerline of the tunnel and therefore be on line with the pitch axis of the downstream airfoil (generator aspect ratio of 3); the tip of the other generator would be 0.5 c above the downstream airfoil (generator aspect ratio of 2). Two electrodes were placed on each vortex generator. One of the electrodes was located on the pressure side of the generator; it extended over 80% of the chord in a streamwise direction and was inboard from the tip a distance of 0.1 c. This electrode was used to visualize the tip vortex. By generating bubbles on the pressure side and allowing them to be advected around the tip to the suction side, the authors believe that a more accurate picture of the coalescing and shedding behavior of the tip-vortex core is obtained. The second electrode was located on the suction side of the generator, extended over 1.3 cm in a spanwise direction, and was upstream from the trailing edge a distance of 0.2 c. This electrode was used to monitor flow separation on the generator. A third electrode was attached to the tip of the generator at the quarter-chord location, and was stretched across the flow to a connection point on the lower test-section window. The purpose of this electrode was to visualize the helical structure of the vortex outside the core region. The pitch axes of both the generator and the airfoil were located at their respective quarter-chords, and a distance of four generator-chord lengths separated the two axes (Fig. 4). This arrangement provided a vortex maturation distance of 2.75 c from the trailing edge of the generator to the leading edge of the airfoil.

The spar of the airfoil extended through the test-section windows and was supported by lift and drag transducers on both sides (Fig. 5). One end of the spar was adjoined to an instrumented drive shaft through a torsionally stiff coupling so that airfoil incidence could be set and the pitching moment measured. Static frictional moments imparted by the support bearings and seals were also measured and later treated as load tares. Only quantities relating to the airfoil were electrically instrumented: incidence, lift (both sides), drag (both sides), total pitching moment, and the bearing and seal moments (both sides). After amplification, the signals were either appropriately summed (i.e., total pitching moment minus both frictional moments) and displayed on local monitors or they were transmitted to a remote data acquisition system where they were digitized, averaged, and stored for later processing. It is estimated that both airfoil and generator incidence were set to an accuracy of 0.2° during the test. Lift and drag measurements are considered to be accurate to 0.01 N and the pitching moments to 0.002 N·m.

The bubbles were illuminated by a sheet of light (about 5 cm wide) directed through the upper test-section window and covering a length of 30 cm in the free-stream direction (Fig. 6). Both continuous and flash sources of light were produced over this length. The continuous source of light was provided by a single 1000-W quartz-halogen lamp; the lamp was used for general viewing, as well as for long-duration exposures (20 sec in this experiment). The flash source of light was obtained from a 10,000-W xenon lamp that could either be synchronized to the shutter of a high-speed camera or operated in a single-flash mode with a view camera. A second xenon lamp (not shown in Fig. 6) was directed upward through the lower test-section window to provide an equal amount of illumination from below the airfoil.

The tunnel was operated at two fixed drive speeds during this experiment. With the airfoil set at zero incidence, the dynamic pressures for these two speeds were 0.10 lb/in.^{2} and 0.025 lb/in.^{2}; they are equivalent to Reynolds numbers of 120,000 and 60,000, respectively, based on an airfoil chord of 10 cm. Some reduction in tunnel speed is thought to have occurred when the airfoil was stalled; however, no attempt was made either to measure or account for this degradation.

The scope of the experiment was limited to discrete values of incidence for the generator and airfoil. The airfoil was placed at both positive and negative values of incidence, and at angles ranging from 0° to beyond stall. Three free-stream conditions ahead of the airfoil were considered. First, a control case in which no vortex generator was present. Second, a mild interaction case resulting from a short vortex generator (tip off centerline) being placed in the stream at angles of 0°, 5°, and 10°. Third, a severe interaction case resulting from a long vortex generator (tip on centerline) being placed in the stream at angles of 0°, 5°, and 10°. Lift, drag, and pitching moment measurements on the airfoil were made at Re = 120,000. Flow visualizations were made at both Re = 60,000 and Re = 120,000, with corresponding velocities of 0.58 m/sec (1.9 ft/sec) and 1.16 m/sec (3.82 ft/sec). In the present paper, only flow visualization at Re = 60,000 and load

measurement at Re = 120,000 are presented. The remaining cases are included in Ref. 7.

III. Description of the Theory

The particular theoretical model to be used for comparison with the experimental data is a panel method formulation using Green's theorem. The code is capable of calculating the trajectory of the vortex, as well as the resulting loads on the airfoil arising from the interaction. A detailed description of the method is given in Ref. 8; however, a brief discussion will be presented here for convenience.

The surface of the wing is approximated by a set of flat panels consisting of uniform sources and doublets. The source strength of each panel is determined by the local external Neumann boundary condition and the strength of each doublet distribution is determined from a set of simultaneous linear equations explicitly specifying the internal Dirichlet boundary condition to zero perturbation potential. The wake generated by the flow over the airfoil is also represented by flat panels of uniform doublet singularities. All wake panels along a streamwise column have the same doublet strength as determined by the zero-load condition at the trailing edge heading that column. When the flow is separated from the leading edge, the wake is enclosed by a pair of free-shear surfaces, each having a doublet distribution of linear strength in the streamwise direction and of constant strength in the crossflow direction. The code also provides for a fully coupled boundary-layer calculation in order to account for the viscous-inviscid interaction.

IV. Discussion of Results

Flow Visualization at Re = 60,000

The tip of the vortex generator was located on the centerline of the tunnel and was, therefore, geometrically on line with the pitch axis of the downstream airfoil. The vortex generator was set to three angles of incidence, $\tilde{\alpha}$ = 0°, 5°, and 10°; and for each of these angles the downstream airfoil was varied from -16° to +16° (Figs. 7-9). By placing the generator at 0° incidence, a control case (Fig. 7) was established against which the effects of the vortex on the streamlines around the airfoil could be evaluated. For brevity, the upstream airfoil that was responsible for producing the tip vortex will be referred to simply as the "generator" while the downstream airfoil that interacted with the vortex will be referred to as the "airfoil."

Rotating the generator to 5° incidence caused a weak vortex to be produced (Fig. 8). The hydrogen bubbles that were formed along the electrode on the pressure side of the generator were swept around the tip to form a relatively large vortex core. The bubbles that were produced along the free-stream electrode near the generator tip are seen to form the outer helical structure of the vortex. Since the core of the vortex leaves the trailing edge of the generator at a slightly inboard location, the central portion of the vortex passes above the airfoil even when the airfoil is at a small negative incidence. Furthermore, it appears that the vortex survives its encounter with the airfoil over an incidence range from about -2° to +8°. At +9° incidence, however, the buffeting effects of the separated flow over the trailing edge of the airfoil causes the vortex to become unstable. At +10° incidence the flow separates from the leading edge and causes the vortex to become unstable before reaching the trailing edge of the airfoil. This instability appears to grow until the vortex becomes unrecognizable after passing about one airfoil-chord length into the wake. As the airfoil incidence increases further, the distance over which the vortex can still be recognized behind the trailing edge of the airfoil decreases. Because of the irregular and large-scale structure of the wake behind the airfoil during static stall conditions, the interaction between the vortex and the airfoil should be considered an unsteady process.

The streamlines of the flow ahead of the airfoil are also affected by the presence of the vortex. However, considerable care must be taken when interpreting these results because the vortex imparts a helical component to the flow field, as a result of which the streamline visualizations nowhere represent a two-dimensional cross section of the flow. Accordingly, these results must be interpreted with caution. Considering the airfoil at an incidence of +8°, and comparing the weak-vortex case (Fig. 8) with the no-vortex case (Fig. 7), it is apparent that two major changes have taken place. First, the vortex (which is rotating counterclockwise when viewed along a downstream direction) has lifted the neighboring flow ahead of the airfoil (on the upwash side of the vortex) by one streamline; and second, the separated zone over the rear portion of the airfoil has increased greatly. Comparing this flow with that for the case without a vortex (Fig. 7), and focusing on the airfoil at +10° incidence, suggests that the effect of the vortex is to induce an increase in the angle of attack by approximately +2° (based on the amount of separation present in each case). Recalling that these observations are applicable only to the upwash side of the helical flow, it is important to note that a similar (though not visible) but opposite condition must be occurring on the downwash side. Since the core of the vortex not only appears as a dense band of bubbles, but is central to the vortical motion, an evaluation of its trajectory is more straightforward. The vortex core seems to move inboard from the generator tip as it approaches the airfoil, cutting across the streamlines that occur in the no-vortex case (see Fig. 7 for -8° and +8° incidence); but after reaching the suction peak on the airfoil, the core closely follows the no-vortex streamlines. At an incidence of -2° (Fig. 8), the outer part of the vortex interacts strongly with the flow along the pressure side of the airfoil. The vortex core is still visible, but the outer helical streamlines disappear and instead become a cloud of bubbles. At more negative angles of incidence, the vortex becomes even more disorganized as it is pulled toward the airfoil. When the airfoil is at -8° incidence, the vortex nearly impacts on the pressure side of the airfoil close to the leading edge. However, for more negative angles of incidence, the vortex is driven away slightly from the airfoil surface. In addition, an instability of the vortex core progresses upstream from the wake (at -10° incidence), to the trailing edge (-11°), and finally to a point ahead of the airfoil (-12°).

Rotating the generator to 10° incidence causes a much stronger vortex to be produced (Fig. 9). Although the trend is essentially the same as that observed for the weak-vortex case, certain features can be described with greater clarity because of the more conspicuous behavior of the flow. In comparing the weak-vortex flow field (Fig. 8) with that occurring for the strong vortex (Fig. 9) when the airfoil is at zero incidence, several observations can be readily made. First, the bubbles comprising the vortex core are confined to a more slender filament, no doubt a result of a greatly reduced static pressure along the vortex core. Second, and in keeping with a vortex of greater strength, the streamlines that form the outer helical portion of the vortex are clearly twisting at a much higher angular rate. Third, the core of the vortex continues to leave the generator at about the same slightly inboard position (0.09 c above centerline-grid line), in spite of the difference in vortex strength. With regard to the stability of the vortex core over the positive incidence range of the airfoil, there is no significant difference between the weak and strong vortex cases. The main difference between the two cases occurs in the streamlines ahead of the airfoil. Referring to the +8° of incidence case, for example, the strong vortex (Fig. 9) causes the neighboring flow ahead of the airfoil (on the upwash side of the vortex) to be lifted by two streamlines (compared to the no-vortex case, Fig. 7), whereas the weak vortex (Fig. 8) shifted the flow by only one streamline. In terms of induced separation over the airfoil, the sequence of flows shown in Figs. 7-9 indicates that separation occurs at slightly over 9° in the presence of a strong vortex, at slightly under 10° for a weak vortex, and probably at about 11° when no vortex is present.

With regard to the trajectory of the core of the vortex in the +8° of incidence case, for example, there appears to be no difference between the weak- and strong-vortex cases. Although core instabilities were observed in the weak-vortex case for -4° of airfoil incidence, their appearance is even more striking during the strong-vortex interactions. Whereas the core never quite collided with the airfoil in the weak-vortex case, a direct impingement occurs at -6° of incidence in the strong-vortex case. Direct impingement causes a wide band of bubbles, with no apparent organized structure, to appear in the wake of the airfoil. Continuing to focus on the strong-vortex case, at -8° of incidence some degree of periodicity can be seen in the wake flow after passing over the suction side of the airfoil, and, at -10°, the scale of this periodicity increases. At -11° of incidence, a particularly interesting event occurs. The core of the vortex just ahead of the airfoil appears to undergo a helical distortion that is characteristic of an unstable vortex. After colliding with the airfoil, the flow breaks down over the pressure side of the airfoil and is shed into the wake with a clearly periodic organization (about 11.5 Hz). At -12° of incidence, the location of this presumed vortex instability moves upstream about one half of a generator-chord length ahead of the airfoil. A similar breakdown of the vortex has been reported in a smoke visualization test[9] of a vortex impinging on a downstream airfoil.

Load Measurements at Re = 120,000

Lift, drag, and pitching-moment loads were measured at a Reynolds number of 120,000. Data were taken at 1° increments of airfoil incidence over a range from -16° to +16°. Because of the high density of data points, symbols have been omitted from many of the figures in order to allow a better examination of the curves that were constructed using straight-line connections between the points.

Of initial concern was the unavoidable presence of the generator wake and its possible effect on the loads of the downstream airfoil. Although the greatest disturbance to the flow field by the trailing-edge wake is created when the generator is placed at maximum incidence ($\tilde{\alpha}$ = 10°), its influence on the airfoil loads cannot be separated from the more dominant effects of the tip vortex. The generator was, therefore, placed at zero incidence in order to produce a wake (albeit small), as well as a distortion of the flow around the tip (but without producing a vortex). The results, which are presented in Fig. 10, show that the presence of the generator in the free stream has essentially no effect on the airfoil loads, even when the generator extends to the centerline of the tunnel. Since some level of disturbance can be expected when the generator is at incidence, the orientation of the generator in the flow field with respect to the downstream airfoil in the present experiment has the advantage of placing the wake farther away from the airfoil than the vortex.

Placing the generator at incidence can be seen to have a definite effect on the airfoil loads, especially when the vortex makes a close encounter with the airfoil (Fig. 11). The vortex causes the airfoil to experience an early stall and a reduced (more narrow) drag bucket. Note that only the pitching moment shows any significant change at angles below stall. This is probably caused by the presence of a laminar separation bubble, which becomes distorted so as to cause only a shift in the center of pressure. The behavior of this bubble, which no doubt is responsible for the kink in the lift curve and the nonzero slope in the moment curve over the unstalled range, is thought also to cause the stall to be different from what is observed at higher Reynolds numbers.[10-12] Although the proximity of the vortex to the leading edge of the airfoil is quite dependent on the sense of the airfoil incidence, the vortex passes over the suction side of the airfoil at the point of stall and causes the same degree of early stall for both positive and negative values of incidence. Based on the onset of lift and moment stall (which appear to be more distinct than drag stall), the interaction causes an early stall by 1.6° in the weak-vortex case and by 2.3° in the strong-vortex case.

When the generator is off centerline, a more modest encounter with the airfoil results (Fig. 12). The effects of the vortex interaction are greatly reduced over the unstalled region, but the same trends are observed as in the strong-interaction case (discussed above). Although there is a difference in the post-stall curves depending on whether the airfoil is at positive or negative incidence, it is interesting that the angle at which stall occurs does not appear to be affected by which side of the airfoil (pressure or suction) the vortex is

on. The most significant difference probably appears in the sense of the rolling moment; however, this quantity was not measured in this experiment. In the present case the interaction causes an early stall by 0.8° in the weak-vortex case and by 1.7° in the strong-vortex case.

Theory at Re = 120,000

In order to better represent the conditions of the experiment, extra panels were added to the formulation to simulate the presence of the upper and lower tunnel walls. All of the computations were made for the close encounter, strong-vortex case. In other words, the generator tip was considered to be on centerline with an incidence of 10°. Comparisons with the experiment were made at three angles of airfoil incidence: α = +8°, +12°, and +16°. The calculated path of the vortex core will be discussed first.

Considering the case for the airfoil at +8° incidence, the computed results are shown in Fig. 13a in the form of streamlines leaving the trailing edge of the generator and passing over the downstream airfoil. The core of the vortex (shown as a dashed line) was computed to be the centroid of the circulation for the vortices in the tip roll-up. The encircled points were obtained from the experiment by making discrete-coordinate measurements along the mean trajectory of the vortex core (from Fig. 21 of Ref. 7). This comparison shows a rather favorable agreement between theory and experiment.

The computation for the interaction with the airfoil at +12° incidence is shown in Fig. 13b. For this calculation, wake-relaxation iterations were required to simulate the flow separation from the leading edge. After three iterations, good agreement with the experimental data was obtained ahead of the airfoil. However, in passing over the airfoil, the agreement remains good only when considering the inner boundary of the band of possible trajectories (the upper and lower boundaries are indicated by the two symbols at each location). Nevertheless, the agreement is classified as being generally good over the entire encounter, since it is beyond the scope of present-day codes to account for this type of unsteady separation behavior. The region of greatest disagreement is just downstream of the trailing edge of the airfoil, where the theoretical core appears to be diverging from that observed in the experiment. This may be attributable to the fact that calculations of the details of the roll-up were terminated before passing downstream of the airfoil.

Examining the results for the final case with the airfoil at +16° incidence (Fig. 13c), the comparison between theory and experiment is not especially good. The calculations made with a "no-separation" restraint agree reasonably well with the experimental results ahead of the airfoil; however, the agreement is poor in the region over the airfoil. A second calculation, which allowed for separation on the airfoil, shows a very different trend; however, the agreement remains poor. Although some of the differences between the theory and the experiment can be reduced by increasing the panel density on the generator[13] as well as by accounting for the initial vortex development over the surface of the generator, it may be that the greatest improvement will come from a better separation model for the flow on the downstream airfoil.

Based on the VSAERO code, the computed lift, drag, and pitching-moment coefficients for the three angles of airfoil incidence are shown in Fig. 14. When the airfoil is stalled, it is clear that the first-iteration calculation (which assumes the flow is fully attached) is incorrect. However, the second-iteration calculation (which allows for flow separation) is in much better agreement with the experiment at +16°. With the airfoil at +12°, the code predicts a partial span separation over the upper surface, whereas the flow was apparently fully separated in the experiment. This difference is probably a result of the level of free-stream turbulence in the present experiment, as well as the strong buffeting character of the stall observed for this airfoil. A partial span separation can occur under certain conditions, as was the case reported in Ref. 14.

V. Conclusions

1) A vortex may survive distortions caused by modest values of transverse and axial pressure gradients more easily than it can shear along its axis.

2) Buffeting from a nearby separated region can initiate a vortex instability, with the path of the core itself assuming a helical shape.

3) An encounter between the vortex and the airfoil boundary layer causes the interacting flow to mix and emerge into the wake with no apparent vortex structure.

4) When the vortex impinges along the stagnation region of an airfoil (and becomes subject to a strong adverse axial pressure gradient), the core of the vortex becomes unstable ahead of the airfoil and is then transformed into a segmented and periodic structure as it moves over the surface of the airfoil.

5) The presence of the vortex was found to cause premature stall in every case in this experiment. The greater the strength of the vortex and the closer the encounter, the earlier the stall.

6) The extent to which early stall occurs appears to be independent of whether the vortex is on the pressure or suction side of the airfoil.

7) The theoretical model considered in this study accurately calculates the vortex trajectory and airfoil loads prior to stall. After stall, calculations for the vortex trajectory do not compare well with the experimental data; however, those for the loads are acceptable.

Acknowledgment

The authors would like to acknowledge and express their appreciation to Rabindra Mehta, T. T. Lim, and Raymond Piziali, who reviewed the original manuscript. They provided valuable challenges to various technical issues raised by the authors, and in so doing, contributed greatly to the readability and accuracy of the final report. The authors would also like to thank Brian Maskew (Analytical Methods, Inc.) for contributing the

theoretical model, for supporting the comparison with the experimental results in an unbiased manner, and for so kindly providing counsel whenever it was required.

References

[1]Smith, W. G. and Lazzeroni, F. A., "Experimental and Theoretical Study of a Rectangular Wing in a Vortical Wake at Low Speed," NASA TN D-339, 1960.

[2]McMillan, O. J., Schwind, R. G., Nielsen, J. N., and Dillenius, M. F. E., "Rolling Moments in a Trailing Vortex Flow Field," NASA CR-151961, 1977.

[3]Cheeseman, I. C., "Developments in Rotary Wing Aircraft Aerodynamics," Vertica, Vol. 6, No. 3, 1982, pp. 181-202.

[4]Ham, N. D., "Some Preliminary Results from an Investigation of Blade-Vortex Interaction," AHS J., Apr. 1974.

[5]Ham, N. D., "Some Conclusions from an Investigation of Blade-Vortex Interactions," AHS J., Oct. 1975.

[6]Maskew, B. and Rao, B. M., "Calculation of Vortex Flows on Complex Configurations," ICAS-82-6.2.3., 13th Congress of the International Council of the Aeronautical Sciences, 1982.

[7]McAlister, K. W. and Tung, C., "Airfoil Interaction with an Impinging Vortex," NASA TP-2273, 1983.

[8]Maskew, B., "Prediction of Subsonic Aerodynamic Characteristics — A Case for Low-Order Panel Methods," AIAA Paper 81-0252, St. Louis, Mo., 1981.

[9]Patel, M. H. and Hancock, G. J., "Some Experimental Results of the Effect of a Streamwise Vortex on a Two-Dimensional Wing," Aeronaut. J., Apr. 1974.

[10]Nakamura, Y. and Isogai, K., "Stalling Characteristics of the NACA 0012 Section at Low Reynolds Numbers," Technical Report of National Aerospace Laboratory, NAL TR-175, 1969.

[11]Nagamatsu, H. and Cuche, D., "Low Reynolds Number Aerodynamic Characteristics of Low Drag NACA 63-208 Airfoil," AIAA 13th Fluid and Plasma Dynamics Conference, 1980.

[12]Mueller, T. J. and Jansen, B. J., Jr., "Aerodynamic Measurements at Low Reynolds Numbers," AIAA 12th Aerodynamic Testing Conference, 1982.

[13]Maskew, B., "Predicting Aerodynamic Characteristics of Vortical Flows on Three-Dimensional Configurations Using a Surface-Singularity Panel Method," AGARD CP-342, 1983.

[14]Mehta, R. D. and Lim, T. T., "Flow Visualization of a Vortex/Wing Interaction," NASA TM-

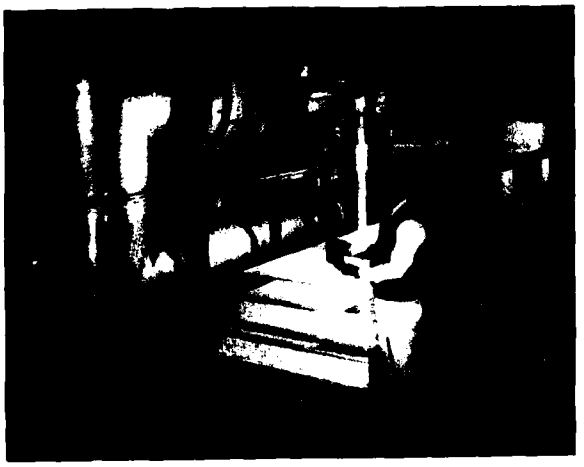

Fig. 1 Aeromechanics Laboratory's 21- by 31-cm Water Tunnel.

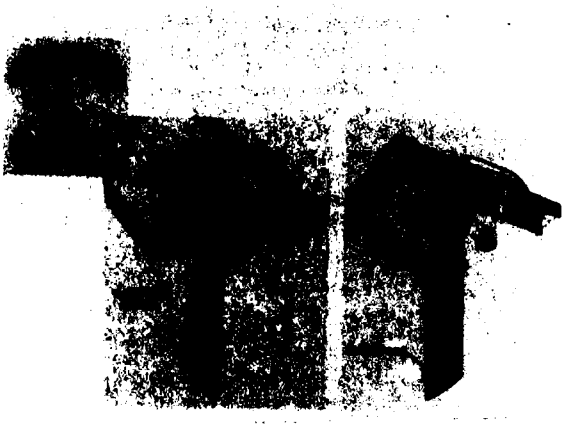

Fig. 2 Mounting of vortex generator on upper test-section window.

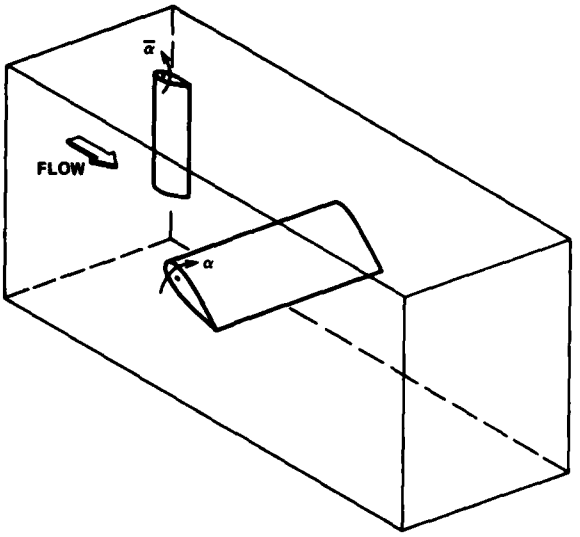

Fig. 3 Orientation of vortex generator and downstream airfoil in test section.

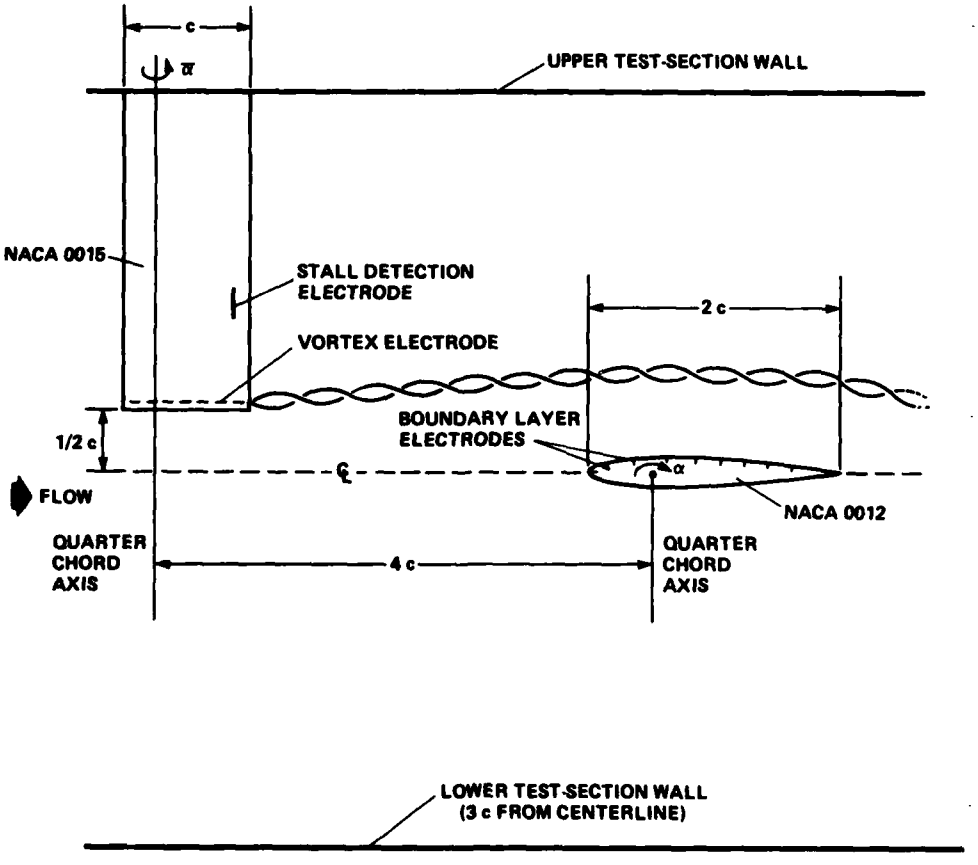

Fig. 4 Relative size and placement of generator and airfoil.

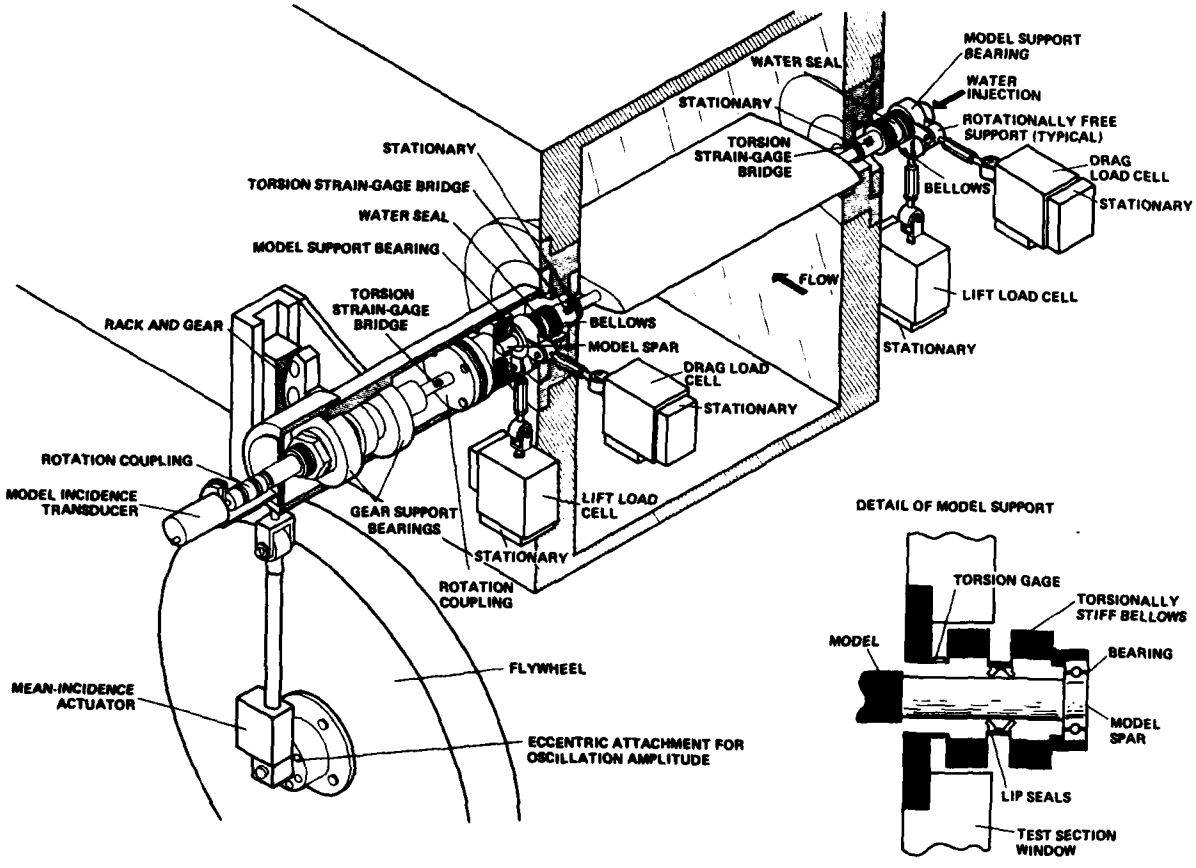

Fig. 5 Model installation and balance system for measuring lift, drag, and pitching moment.

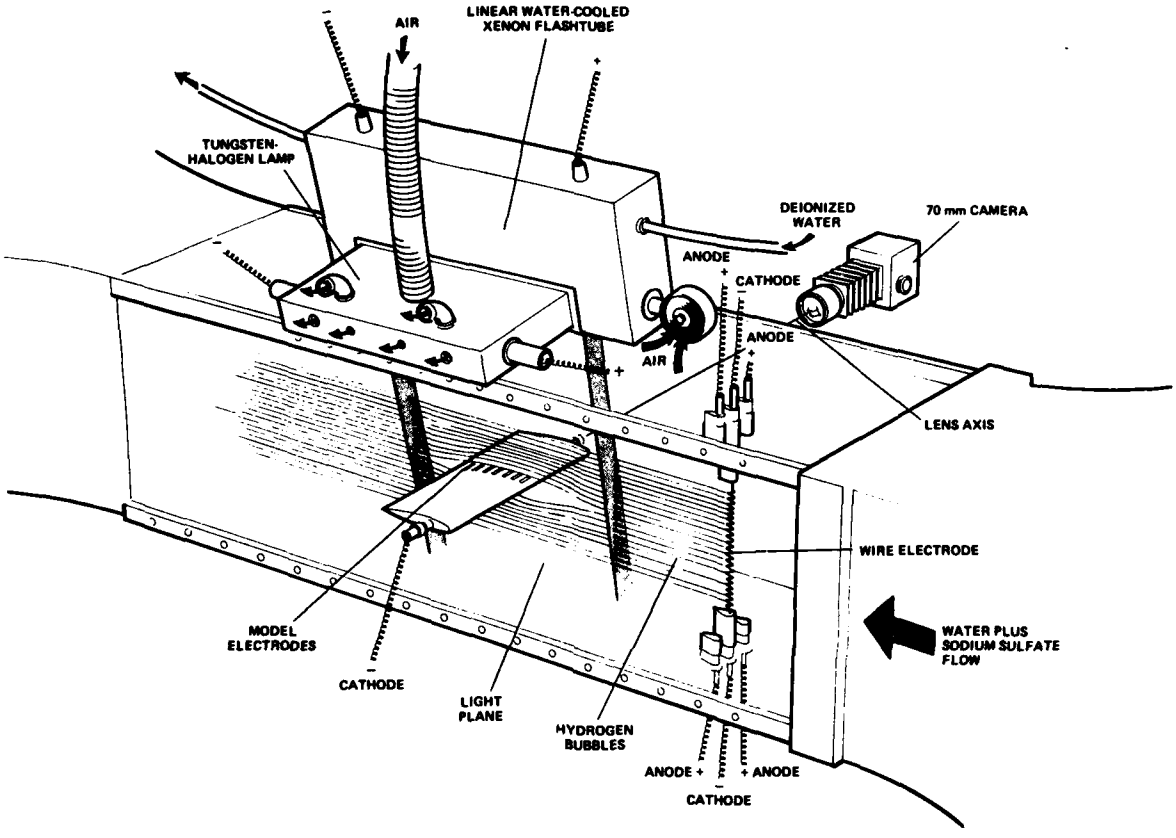

Fig. 6 Lighting system used to illuminate hydrogen bubbles.

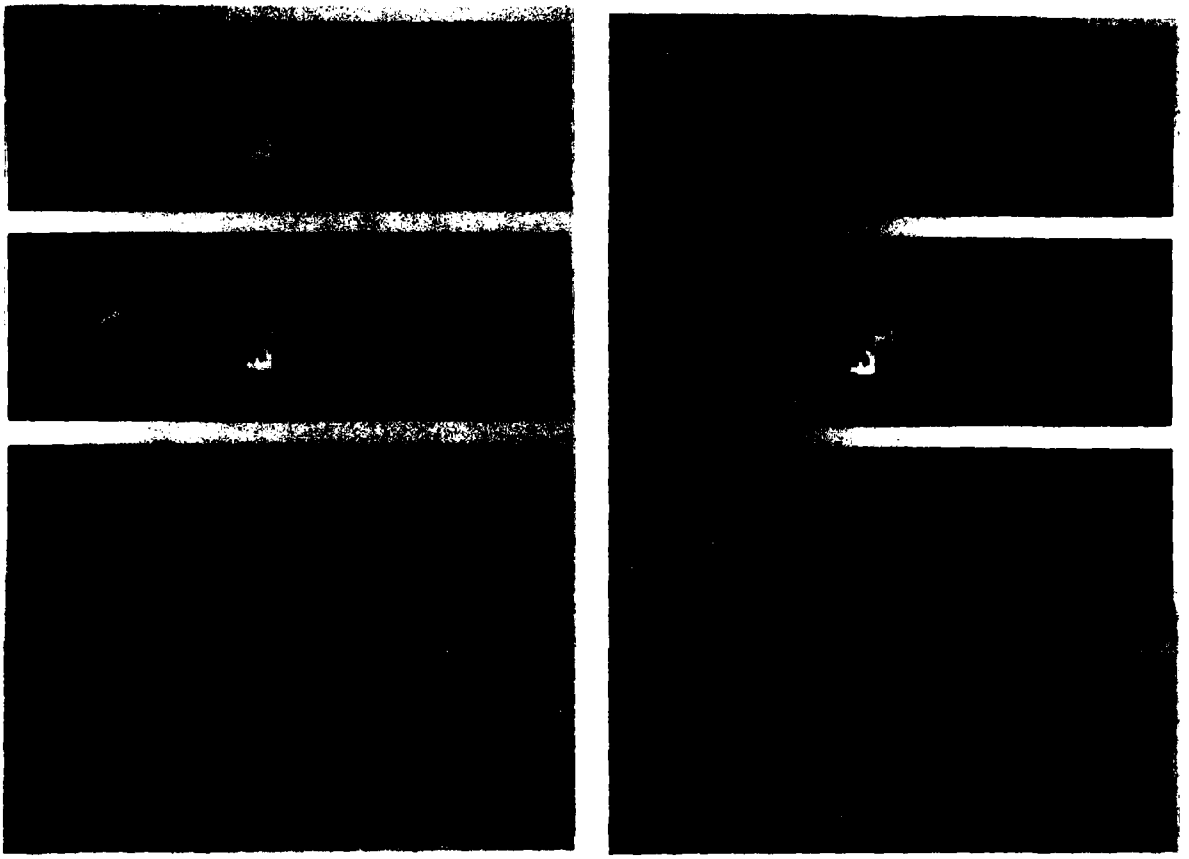

Fig. 7 Visualization of flow at Re = 60,000 with generator on centerline and set at $\tilde{\alpha} = 0°$ (no-vortex case).

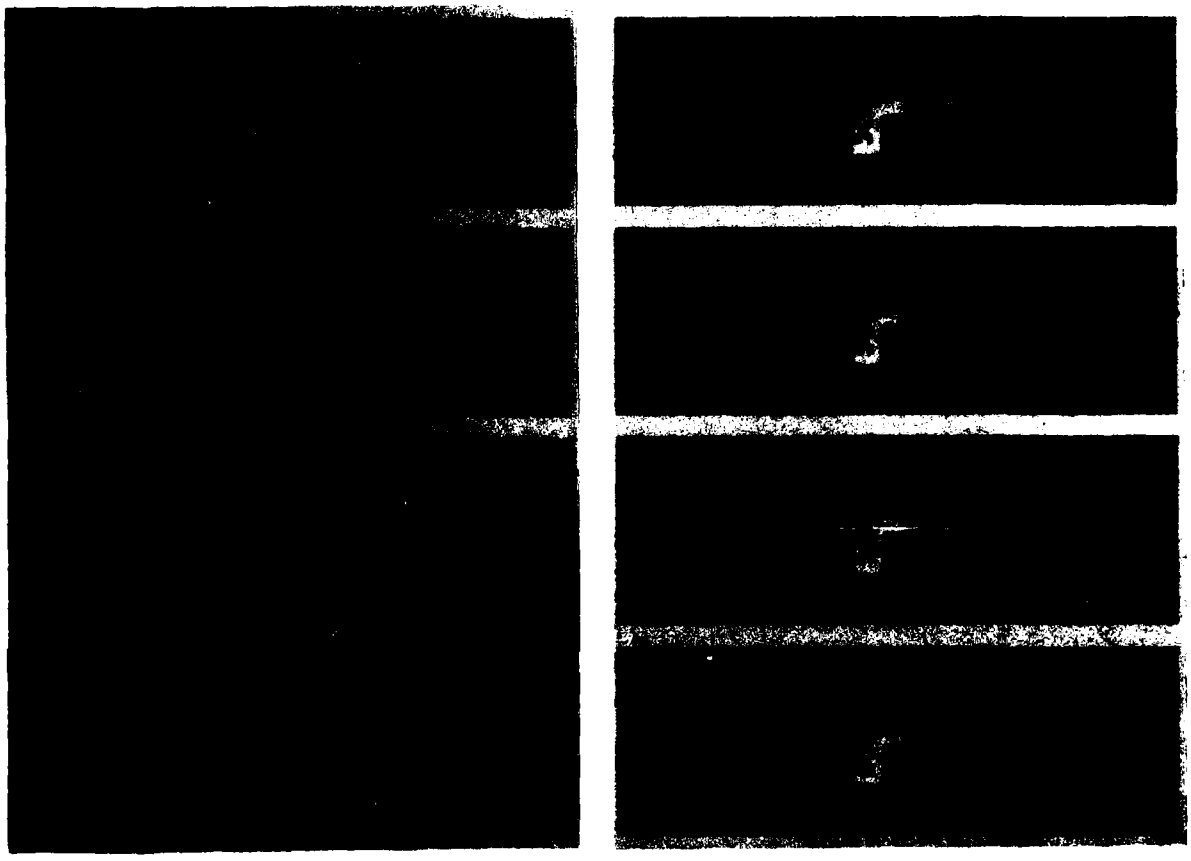

Fig. 7 Continued.

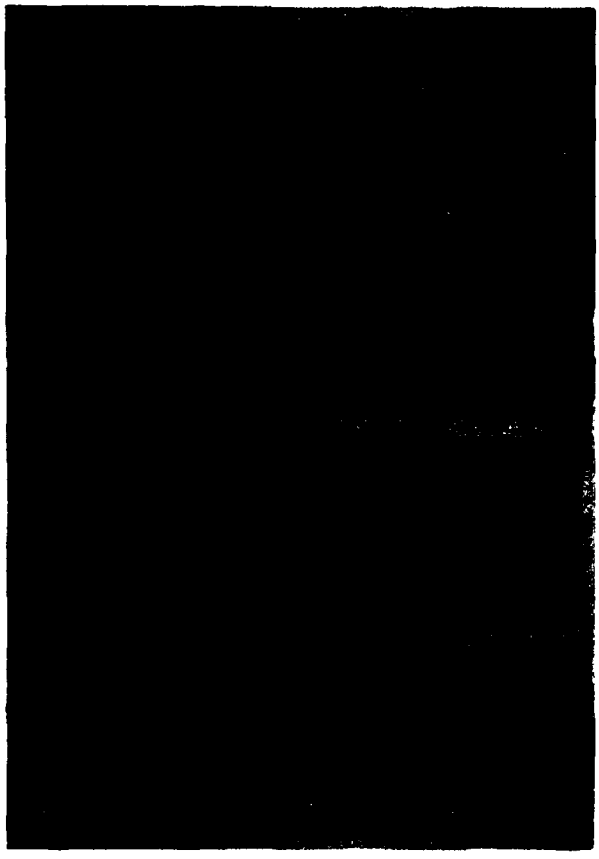

Fig. 7 Concluded.

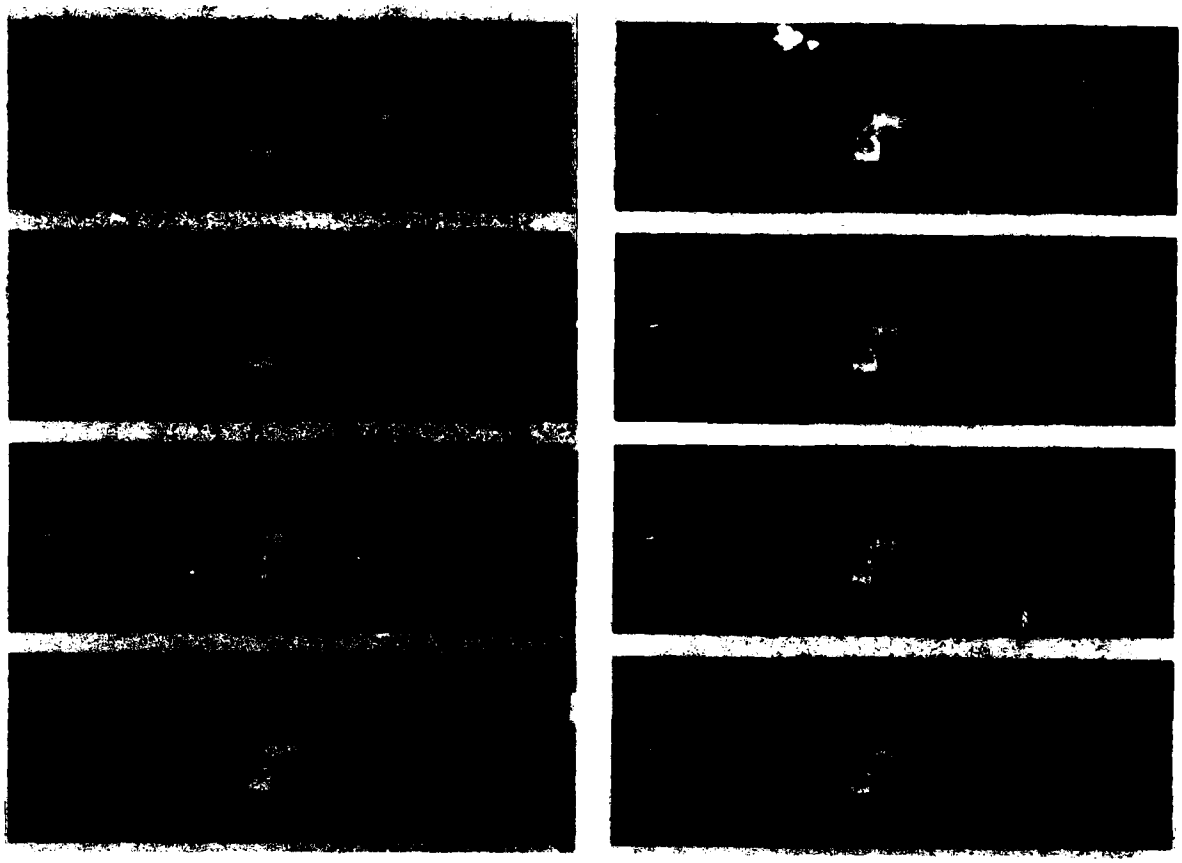

Fig. 8 Visualization of flow at Re = 60,000 with generator on centerline and set at $\tilde{\alpha}$ = 5° (weak-vortex case).

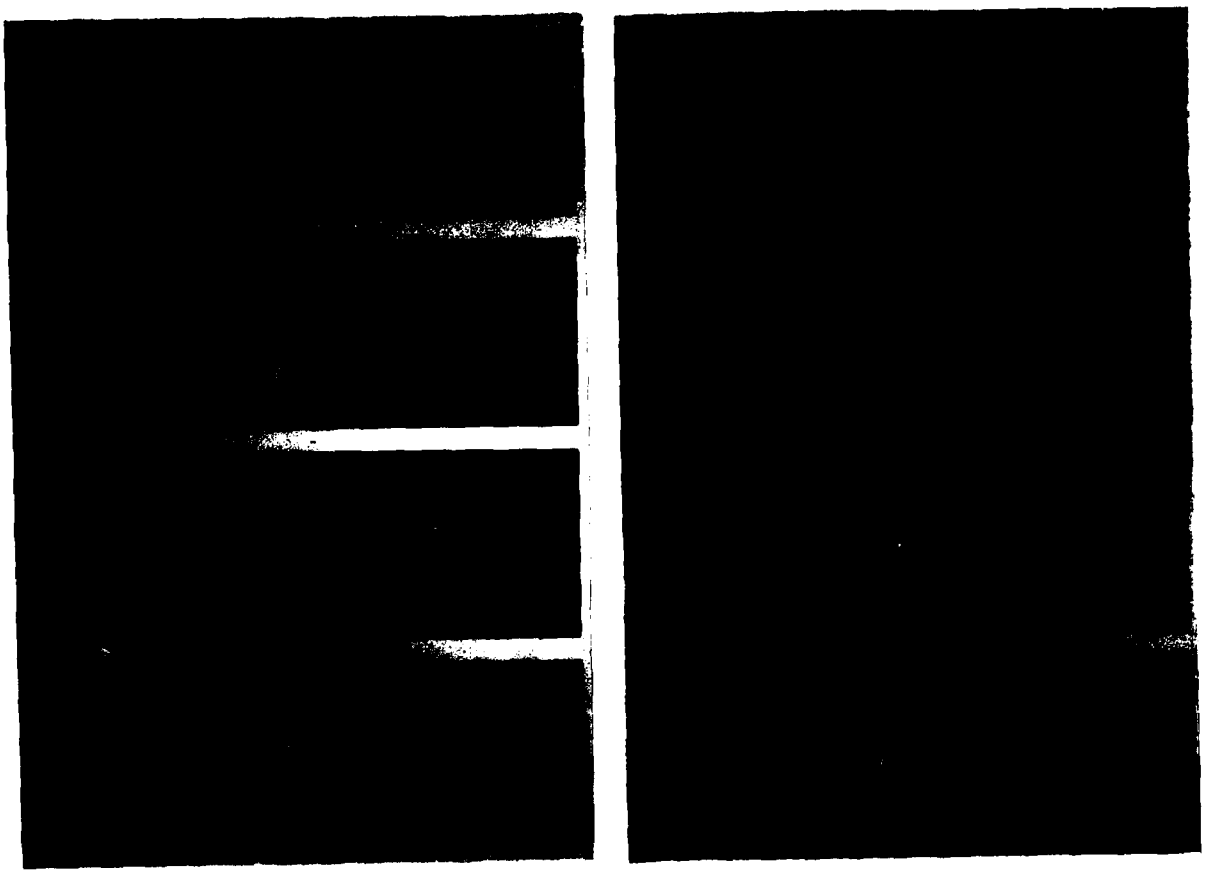

Fig. 8 Continued.

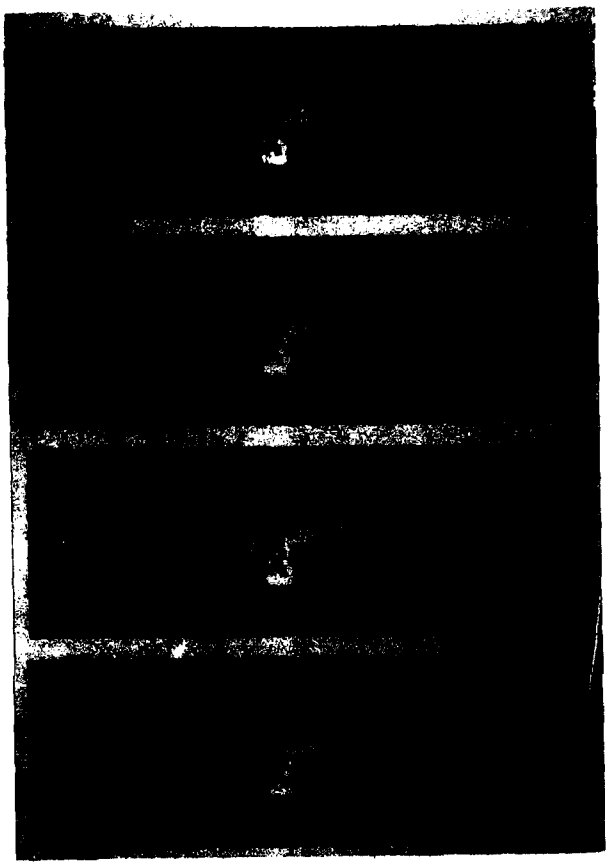

Fig. 8 Concluded.

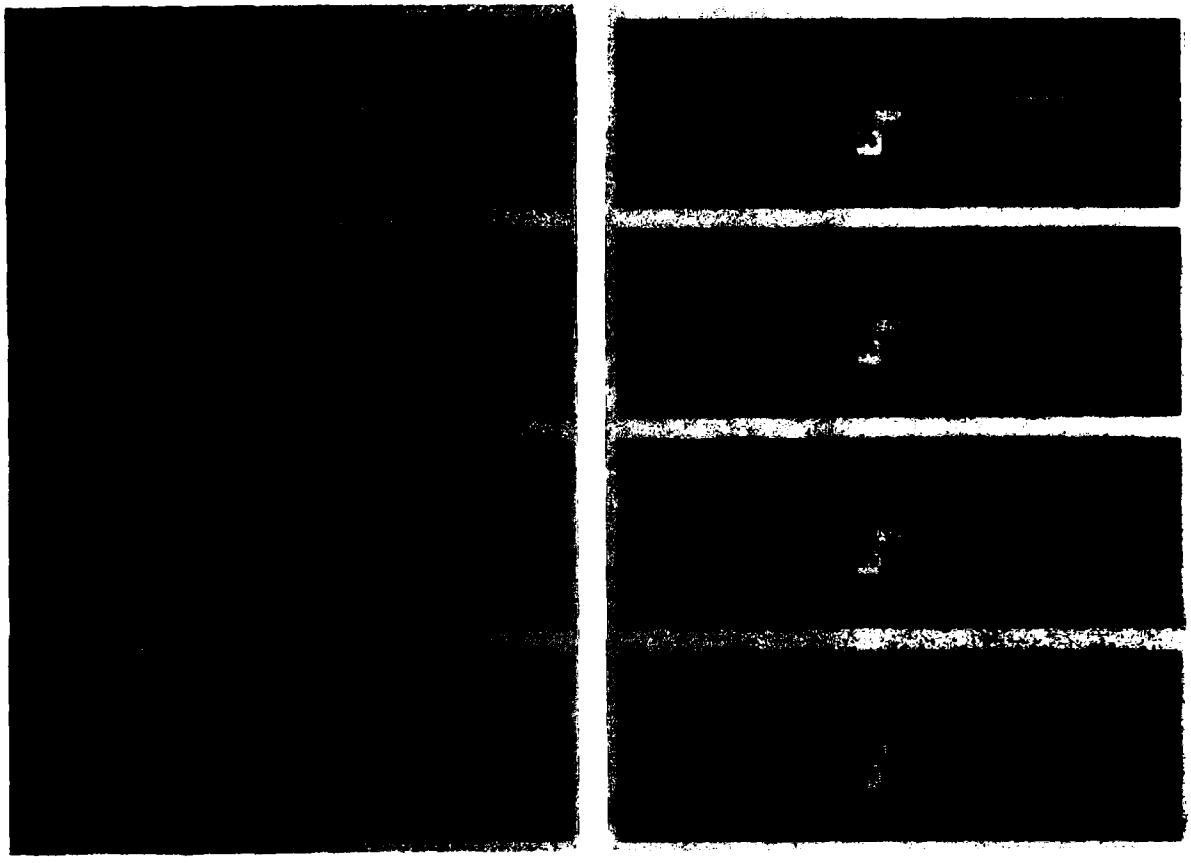

Fig. 9 Visualization of flow at Re = 60,000 with generator on centerline and set at $\tilde{\alpha}$ = 10° (strong-vortex case).

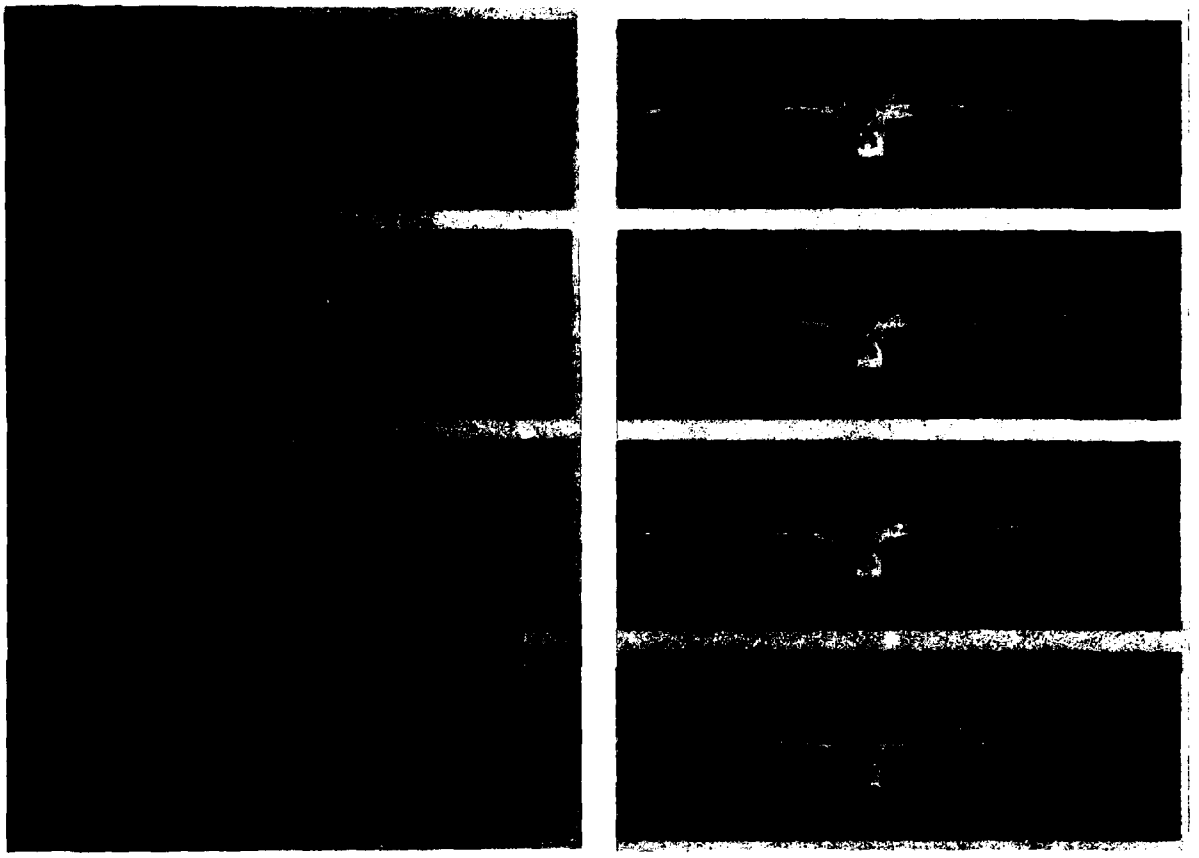

Fig. 9 Continued.

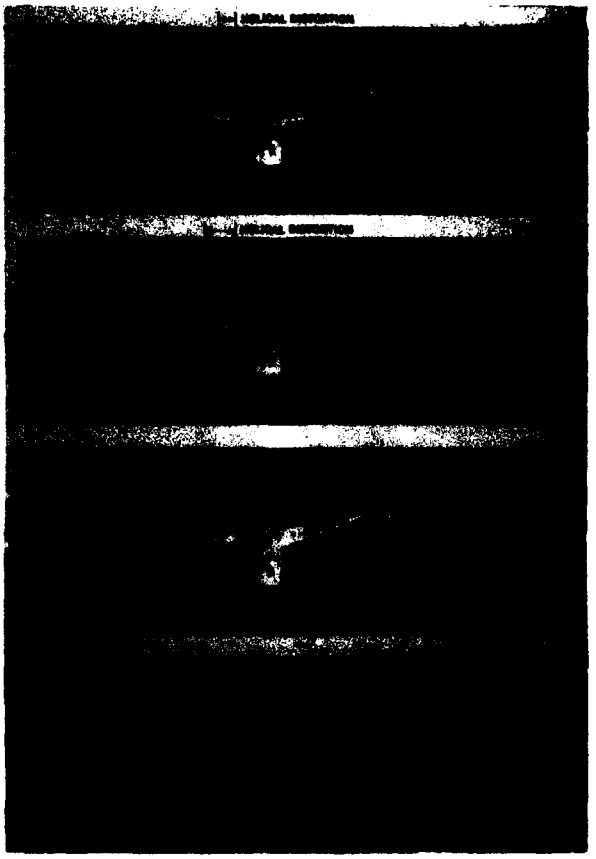

Fig. 9 Concluded.

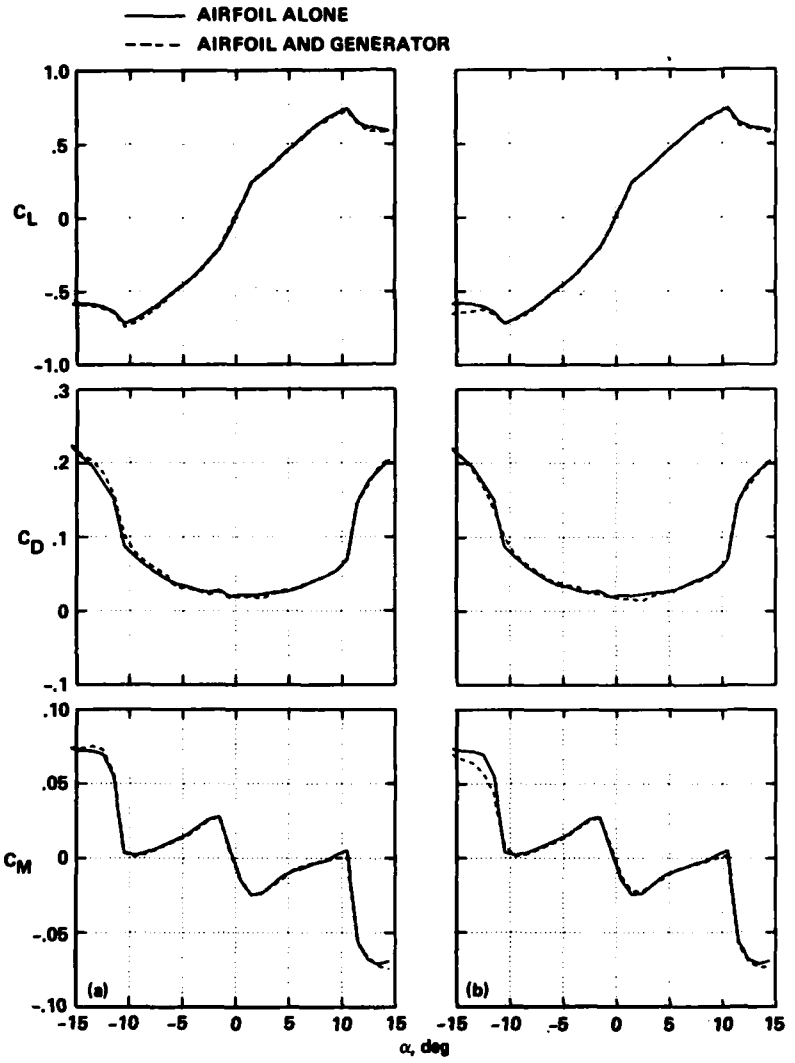

Fig. 10 Generator wake effects on airfoil loads when $\tilde{\alpha} = 0°$.

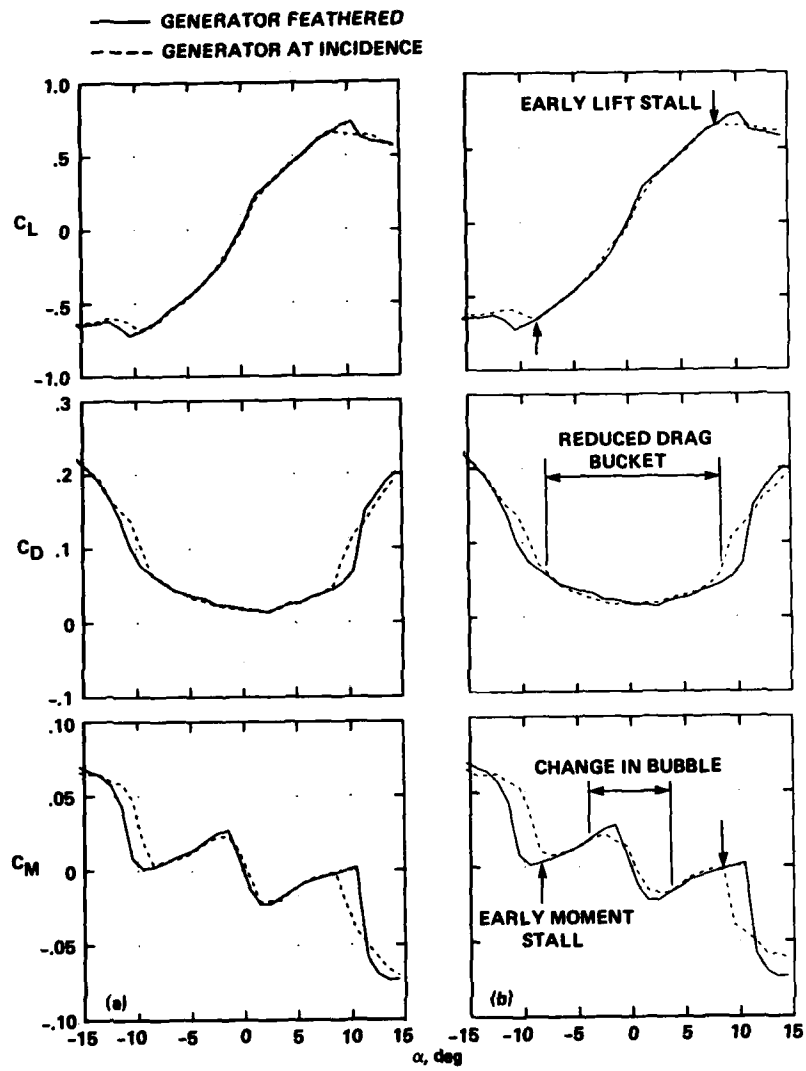

Fig. 11 Airfoil loads during vortex encounter with generator on centerline.

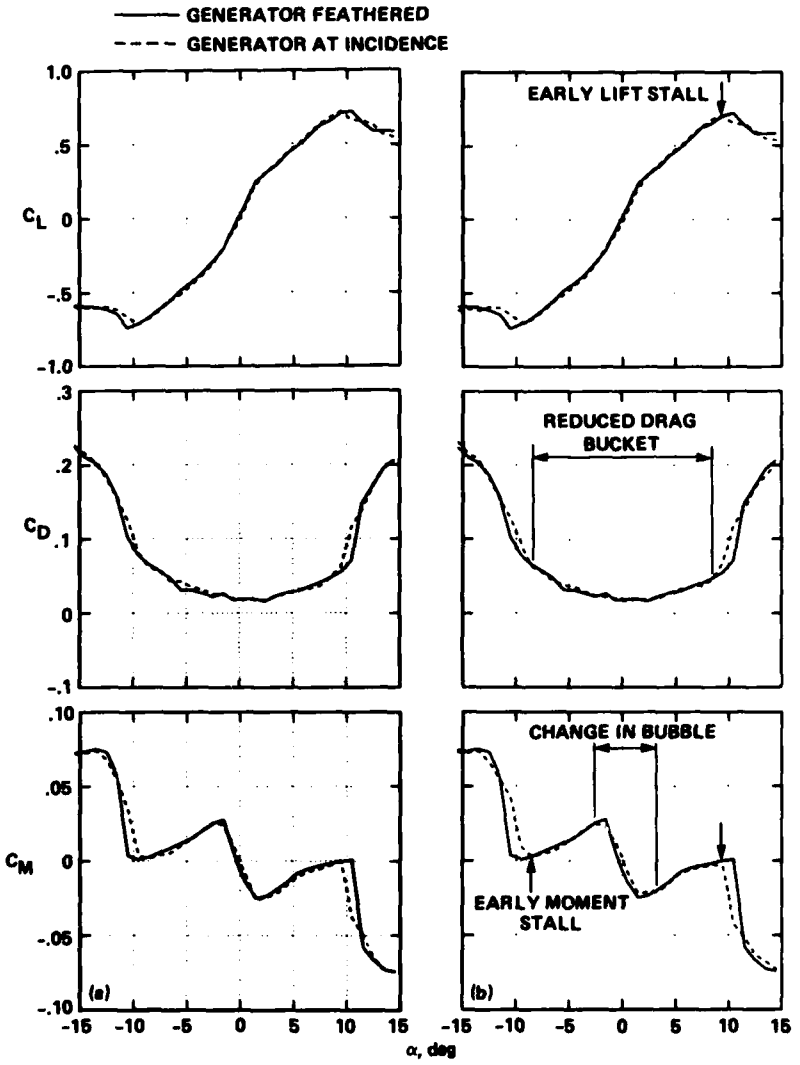

Fig. 12 Airfoil loads during vortex encounter with generator off centerline.

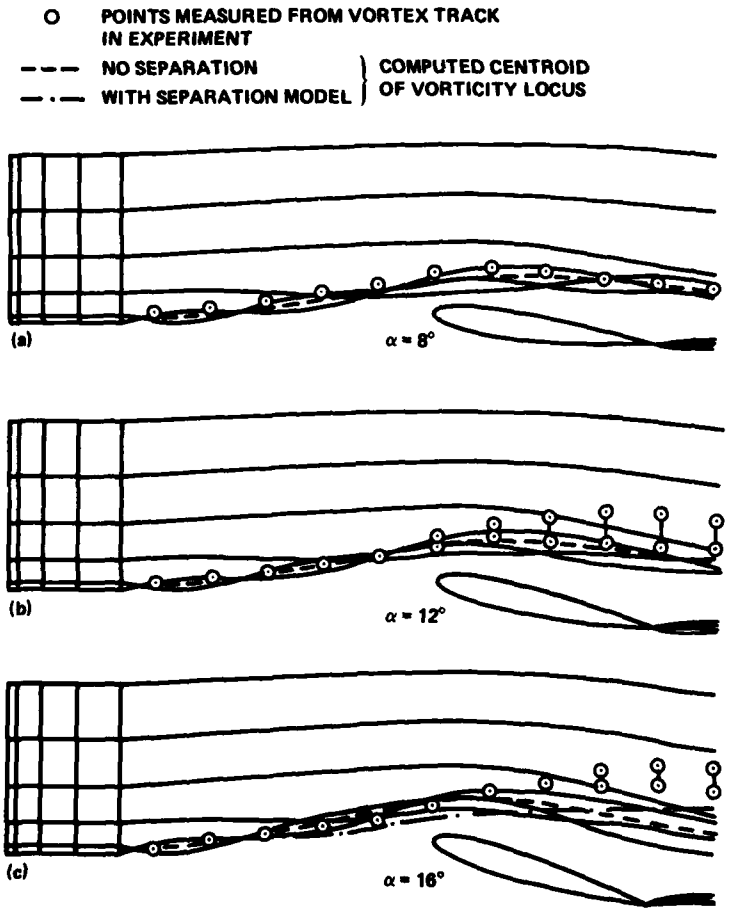

Fig. 13 Comparison of theory and experiment.

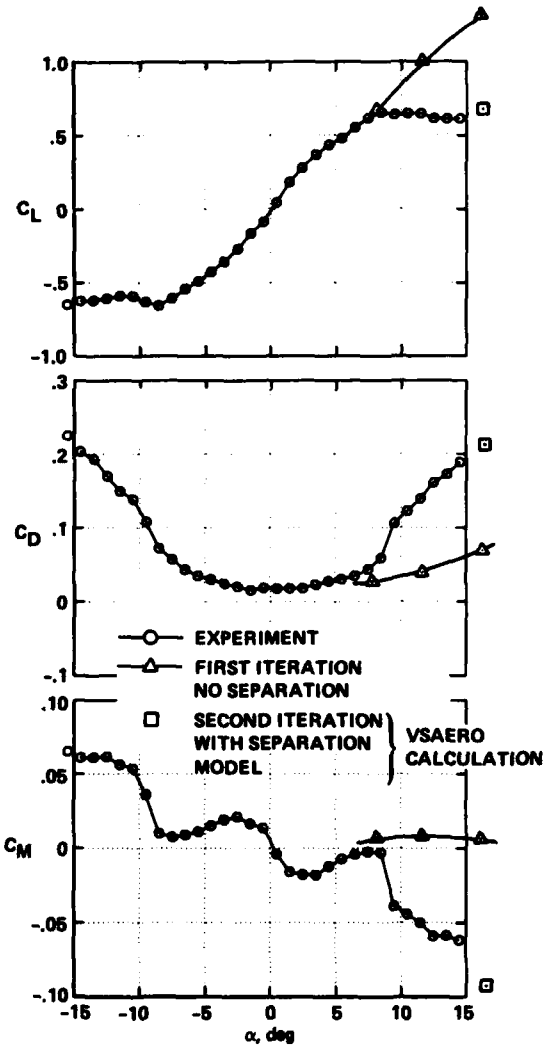

Fig. 14 Comparison of theory and experiment over separated region.

END

FILMED

10-84

DTIC